3 Local Anodic Oxidation

Der Worte sind genug gewechselt,
Laßt mich auch endlich Taten sehn!
Indes ihr Komplimente drechselt,
Kann etwas Nützliches geschehn.

(Johann Wolfgang von Goethe, Faust I)

3.1 Introduction

3.1.1 Overview

A NEGATIVE BIAS applied to the tip of a scanning probe microscope (SPM) can locally oxidize nearby metal or semiconductor surfaces. This anodization process, which is illustrated in Fig. 3.1, is known as local anodic oxidation (LAO) or SPM lithography.[1] It requires that the instrument operate in air under ambient conditions, so that oxide-passivated hydrophilic surfaces will be covered by a thin layer of adsorbed water [1].

After the initial oxide layer has been created, further oxidation requires the migration of oxyanions, substrate cations, or both through the oxide film. The electric field set up in the oxide by the voltage difference between the probe and the substrate enhances their diffusion into the surface. If an SPM probe is brought close to the surface and a bias is applied to it, a water meniscus, which acts as a source of oxygen anions, forms between the tip and the sample [2–4]. As the formation of this meniscus is essential for successful anodization, the

[1] From Greek λίθος, 'stone', and γράφειν, 'to draw'. Originally referring to printing with a limestone, the word has come to mean any pattern transfer technique.

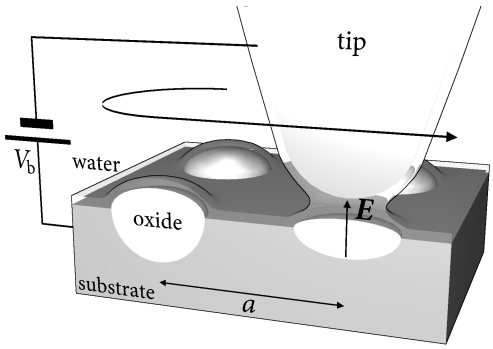

Figure 3.1: Local anodic oxidation

technique depends on the ambient humidity, which affects the thickness and continuity of the adsorbed water layer.

3.1.2 Motivation

LAO has successfully been demonstrated on a variety of materials, including III–V semiconductors. Thanks to improvements in SPM technology, such as feedback mechanisms that reduce drift originating from the creep and the hysteresis of the piezoelectric actuators, the method has evolved to the point where it allows the creation of complex nanoscale features with a resolution comparable to electron beam lithography (EBL).

In contrast to EBL, which will be considered in more detail in Sec. 4.2.2, LAO with an AFM does not suffer from proximity effects and can achieve optimal resolution even for dense patterns [5, 6]. The demands on the instrumentation are not as strict and optimal resolution can be obtained with relatively inexpensive equipment. Moreover, many materials can be manipulated directly, and a separate mask and etching procedure, which can incur damage to the bulk of the substrate, may be avoided. On the other hand, LAO is restricted to shallow etching of a limited number of materials, suffers from a poor reproducibility, and it now appears that the ultimate resolution obtainable by this technique[2] is less than that of EBL.[3]

[2] This is certainly not true for SPM-based lithographic techniques in general

[3] Another limitation, which is of little importance for scientific research and prototyping, but precludes the use of LAO in industry, is the extremely low yield of this technology even if compared to EBL.

The aim of the present work is to investigate lateral modulations of the quasi-two-dimensional carrier gases that form in GaSb–InAs–GaSb double heterojunctions (DHETS). I have set out to evaluate the use of LAO for creating such modulations by removing part of the upper GaSb layer, exploiting the sensitivity of these carrier gases to the proximity of surface states. Chapter 5 discusses the fundamental electronic properties of the DHETS, while chapter 7 considers lateral modulations in the form of antidot patterns and reports on the effect of dot patterns created by LAO on the magnetotransport in these structures.

3.2 Oxide Growth

3.2.1 The Mott-Cabrera Model

LAO is a practical technique for materials that form thin protective oxide layers in the presence of oxygen. In the temperature range where such layers are formed, the oxide growth on these materials starts out quickly but virtually stops after an oxide of finite thickness has been formed. For the materials approachable by LAO, the ultimate thickness is of the order of several nm to several tens of nm. The formation of this native oxide can be explained within the framework of the theory originally developed by NEVILL MOTT and NICOLÁS CABRERA [7, 8].

Discussing this model, I shall follow the usual conventions [8, 9] and assume a quasi-one-dimensional system consisting of:

1. the parent material, *i.e.*, bulk metal or semiconductor, for $x \in (-\infty, 0)$
2. an oxide layer of thickness X in the region $x \in [0, X]$
3. a source of oxygen, *e.g.*, air or water, for $x \in (X, \infty)$.

Once the initial oxide layer has formed, further oxidation requires mass transport through this film, which in general may proceed through diffusion either of ions or ionic defects or of neutral atoms. If no external circuitry is present, electrons and holes must pass through

the oxide as well. In the steady state approximation, the concentration n_s of each diffusing species s is assumed to be constant in time. Particle conservation, in the form of the familiar continuity equation $\partial n_s/\partial t = -\partial j_s/\partial x$, then dictates that $\partial j_s/\partial x = 0$ and the particle current j_s is constant throughout the oxide. One can accordingly write the oxide growth rate as

$$\frac{dX}{dt} = \sum_s \Omega_s j_s, \tag{3.1}$$

where Ω_s is the volume of oxide formed by the transversal of a single ion of species s [9].

According to Mott and Cabrera, the effect of the space charge created by the diffusing charged particles can be neglected for thin oxide layers: The contribution V_ρ to the potential due to the space charge $\rho(x) = \sum_s q_s n_s(x)$, where q_s is the charge of a single ion of species s, can be found from Poisson's equation and evaluates to $(1/2\varepsilon)X^2\rho$ if ρ is independent of x; if $X \ll \sqrt{\varepsilon k_B T/e\rho}$, eV_ρ is small compared with $k_B T$. This condition is typically fulfilled for native oxide films [7–9].

They further assume that electrons are transported through thin oxide films via tunnelling or thermal emission and the electronic motion is rapid compared to the ionic motion. If a layer of oxygen is present at X, some of the oxygen atoms will be converted to O^- ions until the chemical potential is equal on both sides of the oxide. This charge separation causes a built-in voltage V_M across the oxide, which is sometimes designated the Mott potential [10]. The magnitude of V_M may be estimated by $eV_M \approx EA_O + W - \varphi_m$, where EA_O is the electron affinity of oxygen, W the binding energy of the oxygen ion, and φ_m the work function of the parent material; V_M is typically of the order 1 V.

For thin films, the electric field $E = V_M/X$ becomes large and controls the ionic transport. If the particle current j_s of ions of species s obeys the linear relation $j_s = \mu_s E$, where μ_s is the mobility, the assumption of single carrier transport leads to a growth rate [7, 8]

$$\frac{dX}{dt} = \frac{\Omega\mu V_M}{X}, \tag{3.2}$$

which can be integrated to give the well-known parabolic law [7–9, 11, 12]

$$X(t) \propto \sqrt{t - t_0} \tag{3.3}$$

with constant of proportionality $\sqrt{2\Omega\mu V_M}$.

For very thin oxide layers, however, the electric field becomes so strong that j_s is no longer proportional to E. In this case, the relationship between the electric field and the particle current can be derived from the hopping model originally formulated by Verwey [7–9]: Let the distance between adjacent potential minima in the oxide be a and the energy barrier between them U. The classical Boltzmann probability that a particle will move from one site to the next is then $\nu \exp(-U/k_\mathrm{B}T)$, where the attempt frequency ν can be identified with the typical phonon frequency [7–9]. An electric field $E(x)$ lowers the activation energy barrier for movement in the positive x-direction by $\frac{1}{2}aq_sE(x)$. The hopping probability thus becomes $\nu \exp\left\{-\left[U - \frac{1}{2}aq_sE(x)\right]/k_\mathrm{B}T\right\}$ in the forward direction, while the probability for hopping in the reverse direction is reduced to $\nu \exp\left\{-\left[U + \frac{1}{2}aq_sE(x)\right]/k_\mathrm{B}T\right\}$ and can be neglected in the strong field limit $aq_sE(x) \gg k_\mathrm{B}T$. The particle current of species s is therefore given by

$$j_s \approx \frac{n_s(x)}{a}\nu \exp\left(\frac{-U}{k_\mathrm{B}T}\right) 2\sinh\left[\frac{\frac{1}{2}aq_sE(x)}{k_\mathrm{B}T}\right]. \tag{3.4}$$

In the strong field limit, $\frac{1}{2}aq_sE(x) \gg k_\mathrm{B}T$ and $2\sinh\left[\frac{1}{2}aq_sE(x)/k_\mathrm{B}T\right]$ can be approximated by $\exp\left[\frac{1}{2}aq_sE(x)/k_\mathrm{B}T\right]$.[4] Assuming that space charges are negligible, $E(x) = V_\mathrm{M}/X$, $n_s(x) = n_s(0)$ and Eq. (3.4) becomes [8]

$$j_s \approx \frac{n_s(0)}{a}\nu \exp\left(\frac{-U}{k_\mathrm{B}T}\right) \exp\left(\frac{\frac{1}{2}aq_s}{k_\mathrm{B}T}\frac{V_\mathrm{M}}{X}\right). \tag{3.5}$$

For single carrier transport, Eqs. (3.1) and (3.5) imply

$$\frac{dX}{dt} \approx \Omega\frac{n(0)}{a}\nu \exp\left(\frac{-U}{k_\mathrm{B}T}\right) \exp\left(\frac{\frac{1}{2}aq}{k_\mathrm{B}T}\frac{V_\mathrm{M}}{X}\right). \tag{3.6}$$

If transport through the oxide is rate determining, $n(0)$ is approximately independent of the oxide film thickness and determined by interfacial equilibrium conditions [9]. In contrast, if we follow Mott and Cabrera in assuming that the transport in the presence of

[4] On the other hand, if $\frac{1}{2}aq_sE(x) \ll k_\mathrm{B}T$, $2\sinh\left[\frac{1}{2}aq_sE(x)/k_\mathrm{B}T\right]$ is approximately $aq_sE(x)/k_\mathrm{B}T$. By considering the total current between x and $x + dx$, the linear diffusion equation $j_s = -D_s\, dn_s/\, dx + \mu_s E n_s$ is then recovered.

a strong field is very rapid and the limiting step is the dissolution of the ions at the interface, the rate of oxidation is given by

$$\frac{dX}{dt} \approx \Omega N' \nu \exp\left(-\frac{W_i + U}{k_B T}\right) \exp\left(\frac{\frac{1}{2} bq}{k_B T} \frac{V_M}{X}\right), \tag{3.7}$$

where W_i is the heat of solution of the ion, b the width of the energetic barrier it has to overcome, and N' is the sheet density of ions available for dissolution [7, 8]. The derivation is analogous to the argument given above.

In both cases, dX/dt has the same functional form

$$\frac{dX}{dt} = u_0 \exp\left(\frac{-W}{k_B T}\right) \exp\left(\frac{X_0}{X}\right). \tag{3.8}$$

By considering growth to have stopped once $dX/dt \gtrsim u_L$, a limiting oxide thickness X_L can be defined as

$$X_L = \frac{X_0}{\frac{W}{k_B T} - \ln\left(\frac{u_0}{u_L}\right)}. \tag{3.9}$$

Following this argument, the oxide growth will stop at a thickness $X_L \propto X_0 \propto V_M$ provided that $T < W/[k_B \ln(u_0/u_L)]$, in agreement with the observed behaviour of many metals [7,8].

The Mott–Cabrera-model is also applicable to the anodic formation of oxide films in an electrolyte [7, 8] and LAO was originally explained as a straightforward extension to it. In the vicinity of the probe, the applied bias would lead to a larger voltage V dropped across the oxide. The oxide growth would terminate at a larger final oxide thickness X_L in the affected areas [2, 4].

3.2.2 Beyond the Mott-Cabrera Model

Several observations have called this simple model into question.

1. According to Eq. (3.9), the total oxide thickness including any native oxide layer should be determined by the bias voltage. Experimentally, a strong sensitivity to the thickness of the native oxide has not been seen, and on Si, features of similar height have been grown on several nm of thermal oxide as on the thin native oxide using the same (pulsed) bias [4].

2. An increase in the limiting thickness is observed when a modulated bias is used. The magnitude of the increase depends on the material. This effect cannot be explained by the Mott–Cabrera-model of anodic oxidation [3, 4, 13].

3. The very high initial growth rates of tens or hundreds of nm/s observed for LAO indicate a high carrier concentration that is not compatible with MOTT's assumption of negligible space charge and E, n_s independent of x [4].

VERWEY's hopping model of ionic transport can be extended to include the effect of space charge and forgo the steady-state approximation which assumes that n_s is independent of time. Numerical calculations indicate that the effect of a non-negligible space charge is to reduce the ionic current through the oxide [9]. DAGATA [4] suggests that the rapid decline in the oxidation rate should not be attributed to the oxide thickness but to the effect of such built-up space charges. This is consistent with the observed effect of a modulated voltage: Depending on the migrating ion species present in the oxide, the modulation of the field can allow recombination to occur during each cycle and prevent the accumulation of space charge.

3.3 Background

3.3.1 Instrumentation

LAO was originally demonstrated on hydrogen-passivated Si surfaces with an STM operating in air [1]. Anodization of silicon and metals with an STM has been explored by a number of studies [14, 15]. However, in the STM the tunnelling current is the controlling parameter for imaging. Consequently, anodized regions, which have a higher resistance, appear as indentations since the feedback loop has to decrease the tip–sample distance to maintain a constant current. This does not reflect the topography of the sample, as the lower density of the oxide causes these regions to become higher than the surrounding substrate. The interplay between the measurement of electrical and topographical properties not only makes *in*

situ assessment of the grown oxide unreliable, to avoid tip–sample contact and damage to the probe operating conditions have to be chosen that result in ineffective anodization. A large tip–sample distance is needed, which results in limited field enhancement, so that the oxide features are thin and the operating speed is low [15].

The AFM, in contrast, separates exposure and imaging processes and is therefore now the preferred instrument for LAO under ambient conditions [5, 15]. Operation of the AFM as a DFM, *i.e.*, in non-contact or tapping mode, is possible and has empirically been found to yield better resolution and reproducibility than operation in contact mode [3, 15, 16]. This is explained with the smaller forces between probe and sample and consequently reduced wear on the tip. However, the electrostatic force between the probe and the sample (BELAIDI *et al.* [17] have considered this subject in more detail) has a much larger effect on the feedback loop of a DFM than in the case of an AFM operating in the steep repulsive part of the tip–sample potential. Both the average tip–sample distance and the oscillation amplitude decrease as a result of the applied bias [3]. Suitable feedback settings for exposure and imaging are therefore different, and optimal operation might require disconnecting the feedback loop altogether. In this case, it is necessary to explicitly compensate for the sample topography if long continuous oxide lines (as opposed to single oxide dots) are to be created [18].

Setting up a bias voltage between the apex of the tip and the sample surface requires a conducting probe; as the resolution that can be achieved with LAO depends to a large extent on the radius of curvature of the tip, sharp probes are required. Practical considerations favour n^+-Si tips, which can be obtained with an apex radius as small as 10 nm and typically have a resistivity of the order 0·1 Ω m. Tips coated with thin (5 to 100 nm) layers of diamond [10], titanium [2, 3, 10, 15], cobalt [19], gold [16, 20], or platinum [15] have also been used. Coatings reduce the sharpness of the tip and result in a less well-defined apex. Very thin metal layers may readily wear off, even if normal operating conditions keeps the tip–sample force small [10, 16]. On the other hand, metal films improve the conductivity of the probe and protect it from oxidation and, to a limited extent, wear. Consequently, some authors show a preference for coated tips [3, 15].

3.3.2 Materials

Most of the work on LAO originally concentrated on silicon surfaces [1–5,15,16,20,21]; it was noted that hydrogen passivation of Si in HF actually hinders the anodization process and optimal results are obtained with a thin layer of native oxide [2,21]. Minimal feature widths of approximately 40 nm [20] and maximal feature heights of 5 to 6 nm [21] are typical for the LAO of silicon surfaces. Silicon forms a stable oxide, which may be used as an etch mask for pattern transfer [5,15].

Anodization with an AFM has also been demonstrated for thin titanium [2,4,10,13,15,22,23] and aluminium [18, 24, 25] layers. LAO of titanium creates an insulating oxide, and a thin titanium layer can be oxidized completely to form nanoscopic electronic devices. Oxides as narrow as 30 nm and fully penetrating a 7 nm thick layer of Ti have been reported. Using *in situ* monitoring techniques to control the resistance of a metal strip remaining between two oxides, line widths of 10 nm have been realized [22]. A particularly large increase in the oxide height with modulated bias voltage, up to a factor of 4, is seen on Ti [4]. LAO of aluminium layers has been proposed as a means of creating robust etch masks on Si and SiO_2 [24]. Both Al and Al_2O_3 can be removed selectively, allowing for a positive and negative process. This idea will be revisited in Secs. 3.7 and 4.2.4. The full oxidation of Al layers 7 nm thick has been observed, producing features with a minimal width of approximately 10 nm and a height of approximately 3·5 nm.

By oxidizing the GaAs capping layer with an AFM, one can locally deplete the quasi two-dimensional electron gas contained in a shallow δ-doped GaAs–$Al_xGa_{1-x}As$ double heterojunction. The effect has been used to confine the electrons to one- or zero-dimensional areas and to form other nanoscale devices, including antidot lattices such as those discussed in Chapter 7 [6,23,26,27]. SASA *et al.* [28–30] have used LAO to modulate a InAs–GaSb heterostructure either by modifying the InAs layer directly or by completely anodizing a thin GaSb or $Al_xGa_{1-x}Sb$ capping layer and dissolving the oxide in water. Complete oxidation of GaSb caps with a thickness of up to 10 nm has proved possible, and line widths of 200 nm and 100 nm have been achieved on GaSb and InAs, respectively.

3.4 Experimental Setup

A ThermoMicroscopes (now Veeco) AutoProbe M5 SPM was employed for anodization experiments. This instrument uses a scanner operating in a closed loop configuration with a displacement detector to compensate for actuator drift and hysteresis. It is therefore suitable for writing large lithographic patterns, which can take several hours to complete. The SPM was installed on an air table equipped with active vibration cancellation. Air table and microscope were kept in an acoustic enclosure.

The assembly was located in a low-grade clean room; a commercial humidifier was used to control the relative humidity of the entire room. This arrangement was found to provide higher achievable humidity and better stability than an alternative setup based on a bubbler feeding a controlled mixture of dry and humidified air to the acoustic enclosure only.

I evaluated a number of different probes based on sharpened silicon tips (Veeco Ultralever A and B). According to the manufacturer, these tips had a typical radius of curvature of 10 nm and a tip angle of 12°. They were attached to cantilevers with a force constant of 2·1 N m^{-1} (3·2 N m^{-1}) and resonant frequency of 80 kHz (90 kHz). The tips and cantilevers were made from Boron doped n^+-Si with a resistivity of 0·1 Ω m. Apart from bare probes, tips coated with approximately 50 nm of cobalt and 20 nm to 40 nm of gold were tested. Cobalt coated tips, intended for magnetic force microscopy (MFM), were previously found to be useful for LAO [19] and could be purchased from the supplier. Gold coated tips were manufactured in the Clarendon Laboratory from uncoated Si tips in an evaporator.

Samples were fixed to the grounded x–y-stage with adhesive carbon pads. In some experiments, the top of the sample was additionally connected to the stage with the help of a metal clip or conductive silver paint. A bias was applied between ground and the probe. For optimal flexibility, the chip carrying the tip was contacted independently of the standard instrument setup and connected to a computer-controlled relay. The relay switched between ground and an external input, to which a constant voltage supply or function generator could be attached. In line with earlier work [4, 15, 16] a current limiting resistor was connected in

series with the AFM probe. During normal operation, the voltage dropped across a 1 MΩ resistor can be neglected; should the tip make direct contact with the substrate, the damage induced by local Joule heating is limited, as at most 30 μA can flow at a bias of −30 V. All anodization experiments were performed at or slightly above room temperature (28 ± 3 °C).

3.5 Antidot Patterns

3.5.1 Pattern Geometry

The objective of my AFM lithography work was to create a two-dimensional lateral modulation of the two-dimensional electron and hole gases present in a InAs–GaSb double heterostructure as described in Chapter 7. This required the creation of a lattice of sample modifications with well defined unit vectors **a** and **b** and individual diameters d, where $|\mathbf{a}|$ and $|\mathbf{b}|$ are of the order of tens to hundreds of nanometres. Although the creation of rectangular and hexagonal lattices using LAO was demonstrated in principle, the samples considered in this thesis are restricted to square lattices with a lattice constant a so that $\mathbf{a} = a\hat{\mathbf{x}}$ and $\mathbf{b} = a\hat{\mathbf{y}}$.

Although the problem of small antidot lattices with a total size smaller than the coherence length of the carriers in the sample is interesting in its own right [6], this was not the motivation of the present work. In order to measure the electrical properties of the patterned heterostructure, the objective was, instead, to modify the entire area of a Hall bar such as could be easily defined with good reproducibility using standard optical lithography (see Chapter 4). In practice, this means an area of approximately 5 μm × 15 μm or a total of 7,500 dots for a square lattice with $a = 100$ nm. Assuming a realistic oxidation time of 0·5 s per dot, a tip speed of 1 μm/s, and a meandering tip trajectory as shown in Fig. 3.2(a), the exposure of such an area takes approximately 1 h 15 min.

As discussed in Sec. 2.3, the piezoelectric scanner of an AFM is subject to a number of effects that compromise its ability to reliably visit a specific absolute position. These scanner limitations are particularly important when reproducibility over the length and time scales

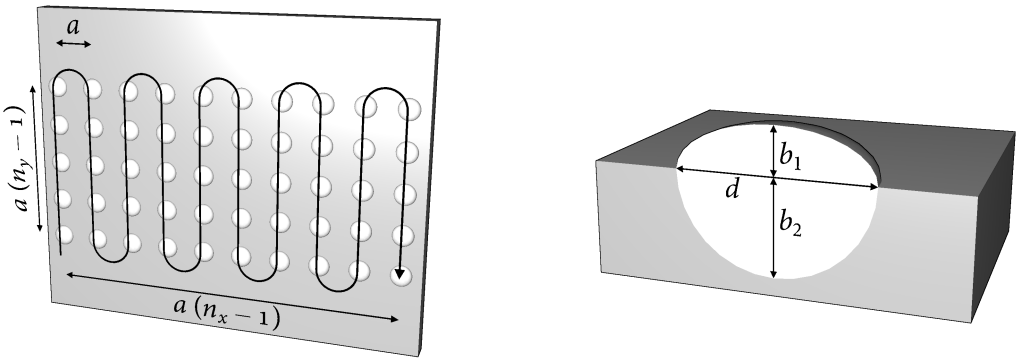

(a) Writing an antidot pattern (b) Simple geometric model of an oxide dot

Figure 3.2: Geometrical considerations for antidot patterns

relevant for the present antidot patterns is required. Operating the scanner in a closed loop setup with independent detectors avoids such problems to a large extent; this is explained in more detail in Sec. 2.3.2. Moreover, as illustrated in Fig. 3.2(a), the smaller extent of a rectangular pattern was chosen as the fast scanning direction for writing if practical, thereby reducing the shift between adjacent rows caused by slow drift. I successfully created patterns consisting of up to 7,500 dots with a local distortion of the unit cell from the nominal shape smaller than the uncertainty of the individual dot positions. No attempt was made to verify the correlation between dot positions in distant parts of the pattern. As the size of the entire pattern is considerably larger than the mean free path of the carriers in the sample, such long range distortions are not expected to significantly affect the electronic properties.

3.5.2 Dot Geometry

The precise shape of the oxide dots is not known. Since the size of the dots is inherently of the same order of magnitude as the radius of curvature of the AFM tip, convolution effects (*cf.* Sec. 2.4.8) are important. Consequently the dot diameter is generally overestimated and the dot profile cannot be determined accurately. Even so, it is reasonable to assume that dots are rotationally symmetric; considering the electric field between a spherical tip and a flat surface [17] furthermore suggests more oxide is produced at the centre and the height of the

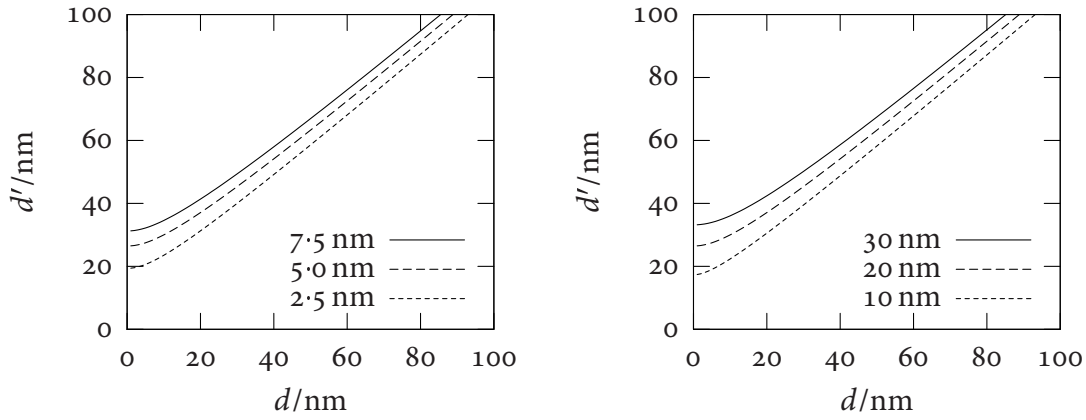

(a) different oxide heights

(b) different tip radii

Figure 3.3: Apparent oxide dot diameter in AFM micrographs, calculated for spheroidal dots with diameter d and height b_1 and idealized tips with a uniform radius of curvature r. The tip radius in (a) is $r = 20\,\text{nm}$ and the dot height in (b) is $b_1 = 5\,\text{nm}$.

dot gradually decreases towards the perimeter. Both assumptions are supported well by AFM measurements within the limitations laid out above.

The dots are most easily described by two half spheroids as illustrated in Fig. 3.2(b). Based on this approximation, it is possible to calculate the size of the dots when imaged with an idealized AFM tip of finite size. The relationship between apparent dot diameter d' and assumed real diameter d is illustrated in Fig. 3.3 for realistic oxide dot and tip sizes.[5] The usefulness of these calculations is limited in so far as the tip size is not generally known exactly and the assumption of a uniform tip radius of curvature may not be accurate.

In the spheroid model of Fig. 3.2(b), the volume of the oxide dot is given by $V_\text{o} = \frac{1}{6}\pi(b_1 + b_2)d^2$, whereas the volume of the oxidized material is $V_\text{m} = \frac{1}{6}\pi b_2 d^2$. If v_o and v_m are the molar volumes of the oxide and the unoxidized material, oxidation of one mole of the substrate yields q moles of the oxide, and the thickness of the native oxide layer is neglected, it follows that

$$\frac{b_2}{b_1} = \left(q\frac{v_\text{o}}{v_\text{m}} - 1\right)^{-1}. \tag{3.10}$$

[5] The calculation is straightforward, but the result involves the solution of a quartic equation, the presentation of which in a closed form is not useful.

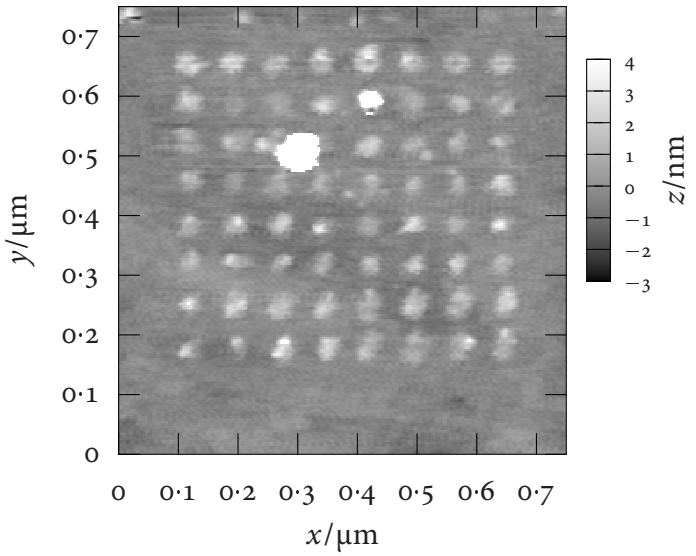

Figure 3.4: AFM micrograph of a square oxide dot array on the free GaSb surface of a GaSb–InAs–GaSb DHET with a nominal lattice constant of $a = 75\,\mathrm{nm}$. The dots have an average diameter of $30 \pm 5\,\mathrm{nm}$ and a height of $4 \pm 1\,\mathrm{nm}$. They were created using a gold coated silicon tip by applying a bias of $-15\,\mathrm{V}$ for 125 ms per dot.

Conversely,

$$q\frac{v_\mathrm{o}}{v_\mathrm{m}} = \frac{b_1}{b_2} + 1. \tag{3.11}$$

These relations hold in fact true for any dot shape as long as $V_\mathrm{upper} = c_1 b_1 d^2$ and $V_\mathrm{lower} = c_2 b_2 d^2$ with $c_1 = c_2$. In particular, if this condition is met the height increase is independent of d and the same as would be expected for a flat surface.

3.6 Local Anodic Oxidation of III-V Semiconductors

3.6.1 Observations

Performance

LAO of GaSb allowed reliable drawing of large arrays of oxide dots with diameters down to $30 \pm 5\,\mathrm{nm}$ and heights of up to $8 \pm 1\,\mathrm{nm}$. Lattices with spacings as small as $a = 75\,\mathrm{nm}$ were realized without any indication of individual sites interfering with each other (Fig. 3.4). The

resolution depends on both the tip and the operating conditions; in practice, the tip determined the achievable resolution, while the operating conditions—within the range suitable for reasonably reliable operation—only had a small influence on the feature size. A limited number of experiments were performed on InAs and GaAs for comparison. If the differences between tips were taken into account, LAO performance was similar on these materials, and no significant difference in the lateral size of oxide dots was observed. Anodization of both InAs and GaAs was generally more reliable than that of GaSb, and oxide dots exceeding 10 nm in height could repeatably be obtained.

Anodic oxide of GaSb can be dissolved in water or dilute hydrochloric acid without attacking the bulk semiconductor [28]. Deoxidation revealed a depth b_2 of the oxide dots between $1{\cdot}0b_1$ and $2{\cdot}0b_1$, which indicated a volume expansion of 1·5 to 2·0 according to Eq. (3.11).

In most cases, lithography was performed on GaSb epilayers grown by metal-organic vapour phase epitaxy (MOVPE) in Oxford within a month of the growth process. Some experiments used MOVPE-grown samples or commercially obtained 'epi-ready' wafers that had been in storage for over a year. Both the height of the oxide features and that of the holes left after oxide removal were comparable for both sets of samples.

The Influence of the Tip

The condition of the probe had the most pronounced effect on the shape and size of the oxide features. In many cases, tips instantaneously changed in such a way that the diameter of the dots that they created increased in size from approximately 30 nm to several hundred nm. Individual dots would then consist of a number of oxide lumps and a 'rubber stamp' behaviour was observed in which this pattern repeated itself at each dot, as illustrated in Fig. 3.5(a). The repeated features in Fig. 3.5(a) evidently resulted from the shape of the tip during anodization, not during imaging: When the shape changed, it did so from one *dot* to the next, not from one (horizontal) *scan line* to the next, as would be expected if the effect were caused during data acquisition. While shadowing was sometimes observed, imaging properties were more often not noticeably affected. On occasion, tips also failed catastroph-

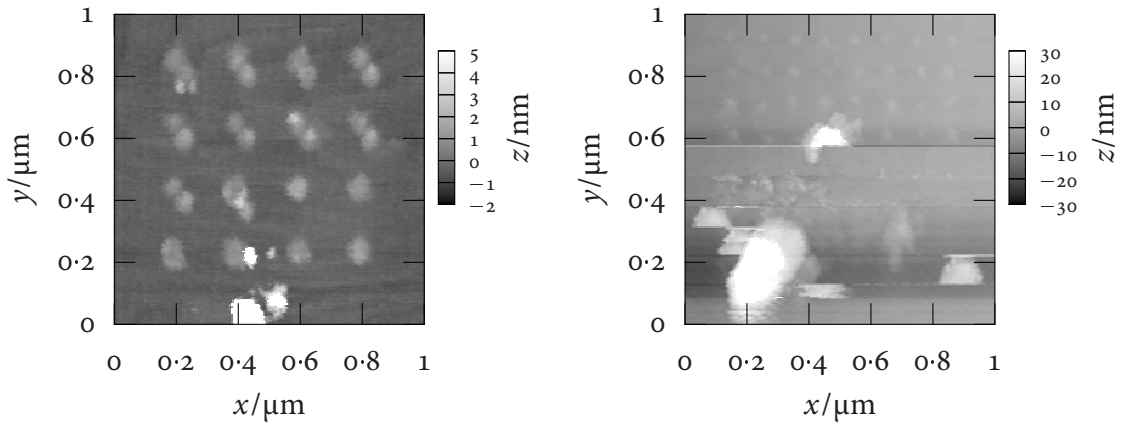

(a) Rubber stamp effect

(b) Tip contamination

Figure 3.5: AFM micrographs of oxide dot arrays on GaSb, showing the effect of tip contamination on LAO. (a) A square array with a lattice constant of 200 nm. The tip was damaged during use and then produced large dots with a complex shape, creating a 'rubber stamp' effect. At the bottom of the plot reversal of the tip change can be observed. (b) A square array with a lattice constant of 100 nm. The tip failed catastrophically halfway through the run, which proceeded from the top to the bottom of the image.

ically, as shown in Fig. 3.5(b). This was accompanied by the creation of large mounds and holes of sizes up to a few micron. Afterwards, these tips either continued to produce such features or created very wide dots indicative of blunt tip apices, which was consistent with the observed imaging artefacts. Finally, some tips started to create increasingly low dots and ultimately ceased to produce any oxide features at all. Such probes occasionally reverted to a usable condition either spontaneously or after forcefully making contact with the sample surface.

Uncoated silicon tips were less likely to lose their lithographic resolution; the behaviour of different new tips was consistent, with some variation in the lithographic resolution. However, they would often stop working after a few days of use. Cobalt or gold coated probes were more prone to instantaneous failure, but less susceptible to aging, which was however still observed for some probes. A gold coating of 10 to 20 nm did not significantly affect either the resolution or the speed at which the oxide grew. Commercially obtained cobalt

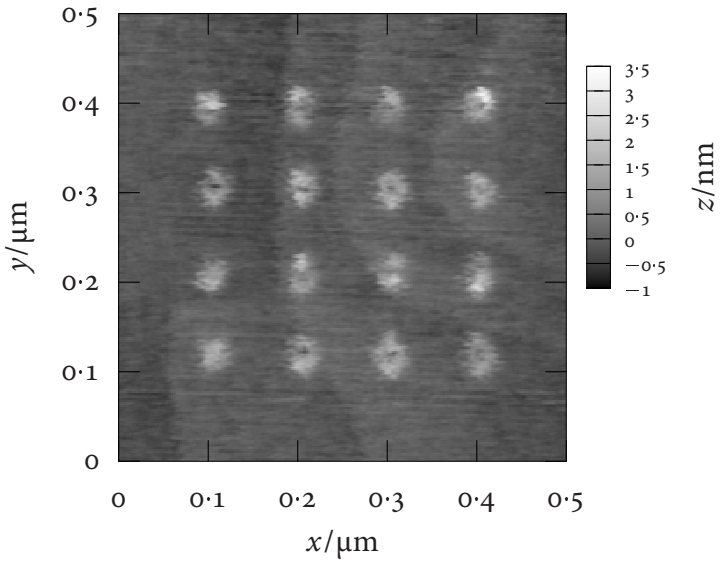

Figure 3.6: AFM micrograph of a square oxide dot array on GaSb with a nominal lattice constant of $a = 100\,\text{nm}$, showing the central indentations observed on some oxide dots. The curved lines correspond to atomic terraces.

coated tips, on the other hand, had on average a worse resolution and required up to 3 s per dot for the oxide height to saturate, as opposed to less than 1 s for the gold coated variant. All probe varieties were used successfully in both contact mode and non-contact mode (NCM). It sometimes occurred that a particular tip ceased to produce oxide features in NCM, but could still be used in contact mode.

Oxide dots frequently showed an indentation at their centre, as demonstrated in Fig. 3.6. Such an indentation could be observed for all substrate materials, but was more pronounced on GaSb. The effect was generally associated with tips that produced wide dots but had a good imaging resolution.

Current and Voltage

A straightforward check of the current between tip and sample was made using a source measure unit (SMU) as the pulse generator. Although the current was normally less than the

detection limit of approximately 10 nA,[6] currents in excess of 10 µA could be drawn if the tip failed or came in contact with the side wall of a large surface feature.

Depending on the tip and operating parameters, there was a threshold voltage in the range 6 to 10 V (negative tip) below which oxide formation did not occur. For voltages exceeding 20 V, the probability of tip failure increased rapidly, which put an effective limit on the oxide thickness that could be achieved with this method.

Motivated by the increased aspect ratio reported as a result of using a modulated bias for some substrate materials, in particular titanium [3, 4], I investigated the effect of modulated voltages on the LAO of GaSb. A square waveform centred around zero with a peak-to-peak voltage difference of 20 V and a duty ratio of 50 % was used at various frequencies up to 1 MHz on its own or in conjunction with a constant offset voltage. When anodizing for twice as long, modulation frequencies up to approximately 200 Hz combined with a negative DC bias on the tip of at least approximately 8 V created oxide dots very similar in size to those obtained with a constant bias. However, no enhancement of the dot height or the aspect ratio was seen. With a small or no DC bias and at high frequencies, the oxide height was significantly *reduced* compared to the unmodulated case. In all experiments with a modulated bias, the uniformity of the oxide dots was improved and the probability of tip failure resulting in a 'stamp effect' was reduced. After such a failure, the tip reverted to a usable state more readily than without the voltage modulation.

3.6.2 Quantitative Results—Dot Patterns on GaSb

Preliminary Remarks

As described in Sec. 3.6.1, the state of the tip is the one parameter that has the most drastic effect on the lithographic performance. In order to gain insight into the influence of the other operational parameters, special care has to be taken to keep the tip as well-defined as

[6] There are several conceptually straightforward ways to improve the sensitivity, analogous to the current measurement in an STM. As currents during LAO were previously found to be negligible [10, 16] and not a controlling parameter for oxidation [15], I did not explore these options.

possible during the experiment. Even so, the possibility that a change in the tip configuration has happened between measurements cannot be excluded and needs to be considered in the interpretation of the results. Moreover, the numerical values for dot diameters, and, to a lesser degree, heights, should be expected to differ among different tips.

The results in this section were obtained with an unused silicon tip (Veeco Ultralever A) on a polished GaSb wafer intended for epitaxial growth. I have selected the series presented here for consistency and because the absence of obvious imaging artefacts indicates a relatively unchanged tip; it does not represent optimal lithographic performance.

To determine the height of each dot, the mean height of the surface—excluding the patterned area—was subtracted from the highest value measured within the dot. The height is not expected to be affected significantly by systematic errors inherent to the afm, because it is much larger than the scale at which the distance dependence of the tip-sample interaction is relevant and much smaller than the scale at which scanner nonlinearity becomes important. In this range, the instrument can be calibrated reliably. The diameter of a dot at its base was estimated by counting the number of pixels lying higher than two standard deviations of the unpatterned surface and assuming a circular geometry—which was generally well supported by the data. Unlike the height, the measurement of the dot diameter *is* affected by the finite size of the tip—inherently of the same order of magnitude as the dot!—and can only be regarded as a upper limit of the actual size. The problem is discussed in more detail in Sec. 2.4.8; it should result in an approximately constant offset. Finally, the yield was defined as the number of oxidation sites actually producing an oxide dot.

Ambient Humidity

As seen in Fig. 3.7(a–c), both the dot height h and the dot diameter d increased with increasing humidity, while no significant change in the aspect ratio d/h could be demonstrated. The increase could be quantified as 0·47 nm per 10 % for the height and 5·3 nm per 10 % for the diameter, but the limited nature of the data did not allow me to accurately prove or disprove linearity. The most pronounced effect of the humidity was on the success rate shown in

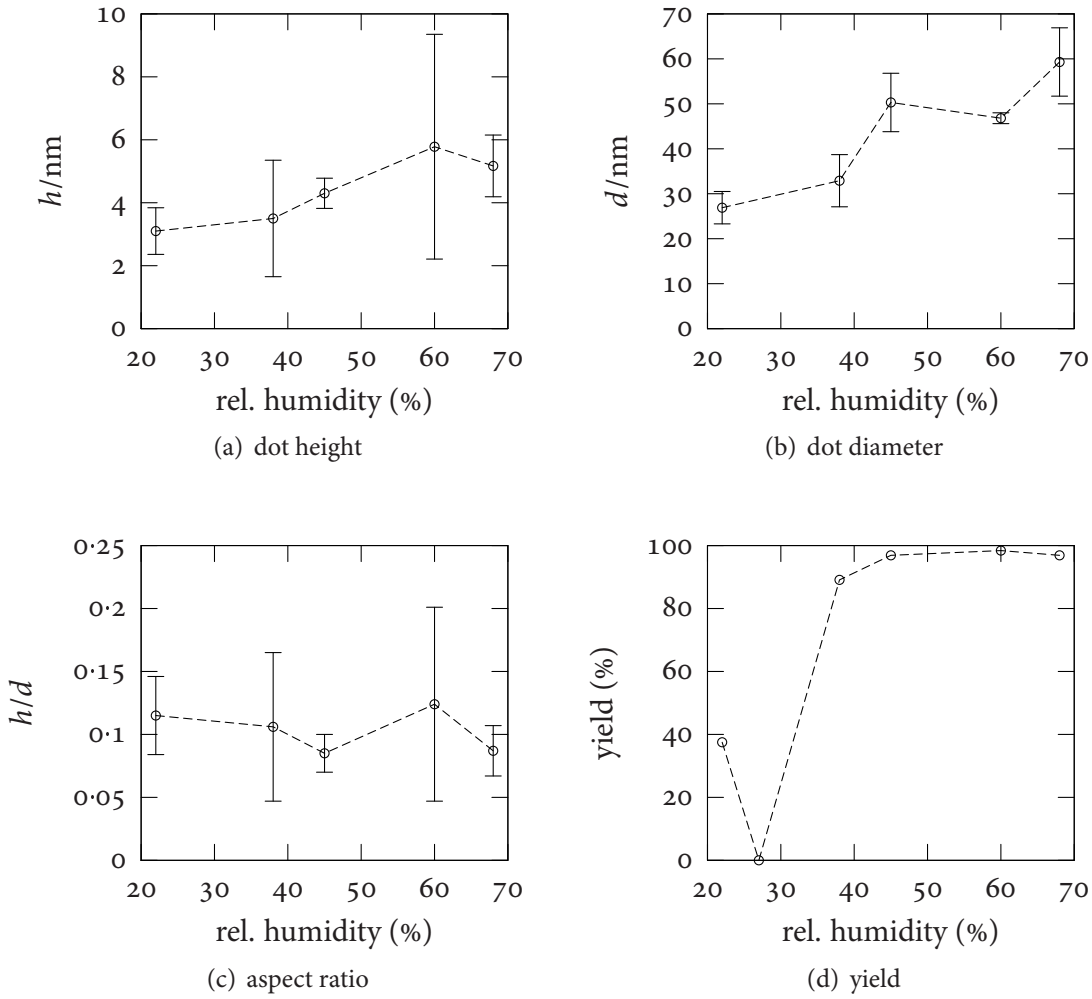

(a) dot height (b) dot diameter

(c) aspect ratio (d) yield

Figure 3.7: Humidity dependence of oxide dot growth on GaSb. 64 oxide dots in a square lattice with lattice constant $a = 300\,\text{nm}$ were grown by applying a bias of $-15\,\text{V}$ to the tip for 2 s. The AFM was operated in 'non-contact' mode with a set point of $-0{\cdot}02$. The data points have been connected with straight lines to aid visualization.

Fig. 3.7(d): At low ambient humidity, only some of the anodization sites showed the development of an oxide dot, whereas the yield approached 100 % for relative humidities exceeding approximately 45 %. The behaviour of the series shown here is consistent with observations made using different tips and operating parameters, although the threshold behaviour was not always as clear.

Bias Voltage

The dependence on the (negative) bias applied to the tip with respect to the sample is illustrated in Fig. 3.8. Both height and diameter of the oxide dots increased approximately linearly with voltage; the height increased by 0·38 nm per V as seen in Fig. 3.8(a), while the diameter, shown by Fig. 3.8(b), was best fit by a line with a slope of 2·51 nm/V. There was a small increase in the aspect ratio, Fig. 3.8(c), with increasing bias. As seen in Fig. 3.8(d), the potential difference had to exceed a threshold of 8 ± 2 V before anodization was observed.

Anodization Time

The dependence of the oxide formation on the anodization time (Fig. 3.9) was characterized by a very high initial growth rate, which decreased steeply with increasing time. The dot height h and the diameter d are shown in Figs. 3.9(a) and 3.9(b). Both quantities appeared to saturate for $t \gtrsim 1$ s. No significant effect on the aspect ratio, Fig. 3.9(c), was detected, and the success rate for oxide formation, Fig. 3.9(d), remained close to 100 % even for short anodization times.

Tip–Sample Distance

The parameter controlling the tip–sample distance in an AFM operating as an amplitude modulation DFM is the amplitude reduction factor (*cf.* Sec. 2.4.5). For the instrument used in the present study, a large negative value of the set point corresponded to a large tip–sample

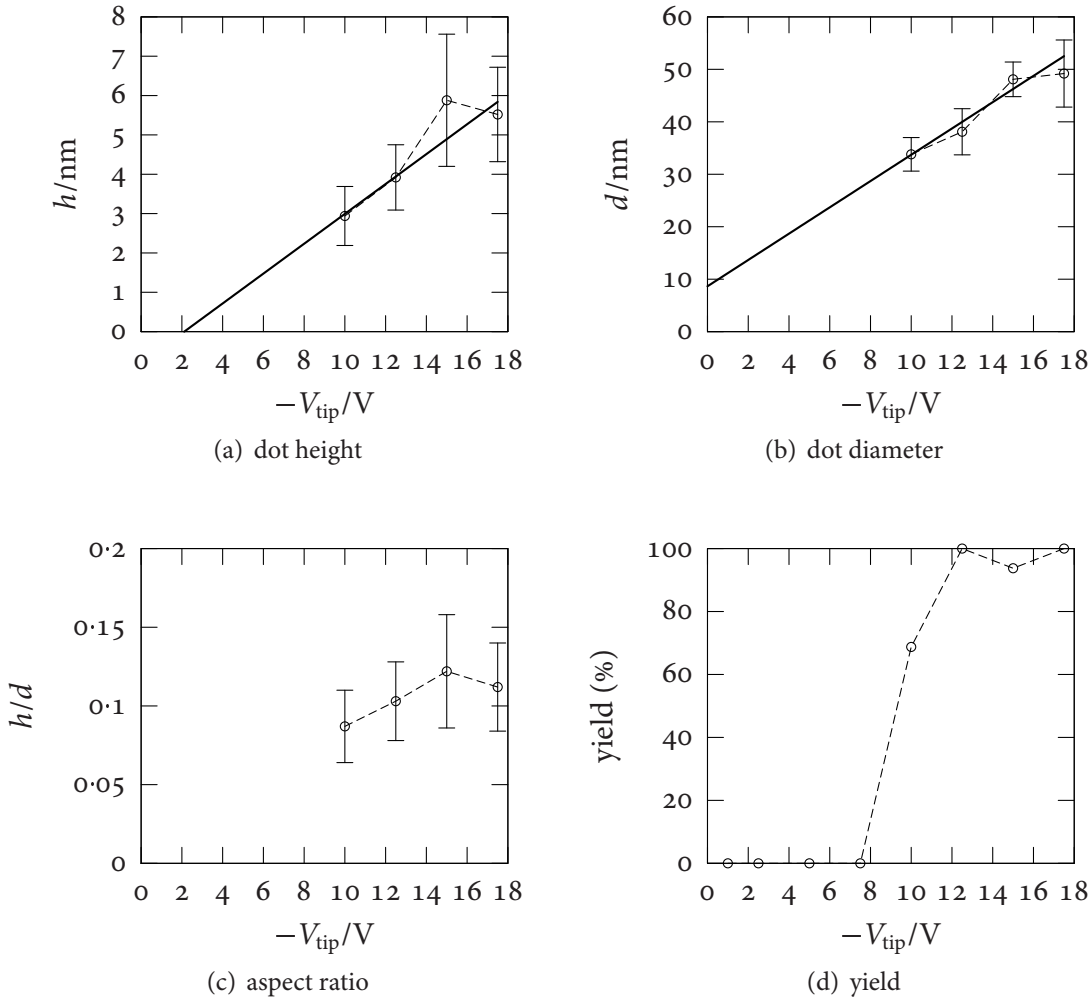

(a) dot height (b) dot diameter

(c) aspect ratio (d) yield

Figure 3.8: Voltage dependence of oxide dot growth on GaSb. Oxide dots in a square lattice with lattice constant $a = 300\,\text{nm}$ were grown at 45 % relative humidity for 2 s. Each data point was averaged over 32 dots. The AFM was operated in 'non-contact' mode with a set point of −0·02. The data points have been connected with straight lines to aid visualization. Thick solid lines are linear fits to the data.

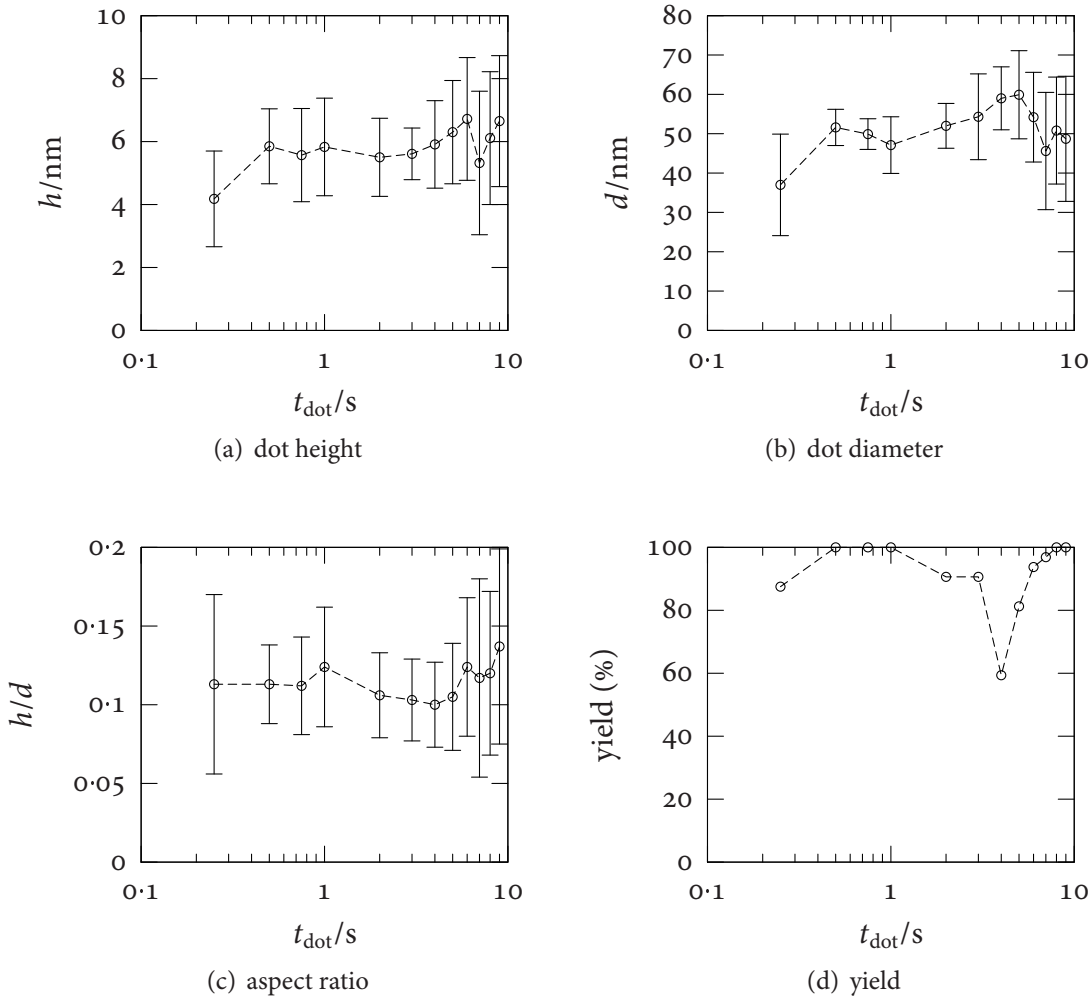

(a) dot height (b) dot diameter

(c) aspect ratio (d) yield

Figure 3.9: Anodization time dependence of oxide dot growth on GaSb. Oxide dots in a square lattice with lattice constant $a = 300\,\text{nm}$ were grown at 45 % relative humidity by applying a bias of $-15\,\text{V}$ to the tip for 2 s. Each data point was averaged over 32 dots. The AFM was operated in 'non-contact' mode with a set point of $-0{\cdot}02$. The data points have been connected with straight lines to aid visualization.

distance. The exact relationship between the set point and the distance depends on the tip-sample interaction and the elastic properties of the cantilever. While the *cantilever* position was fixed during anodization, both the oscillation amplitude and the mean tip–sample distance were affected by the electrostatic force resulting from the bias voltage.

No systematic dependence of the shape and size of the oxide dots on the set point (and hence on the *initial* tip–sample distance) was detected (Fig. 3.10). As seen in Fig. 3.10(d), no oxide dots were formed for large tip-sample distances and a small (negative) set point was required for reliable operation. All set point values used in this study could be used to successfully obtain micrographs of previously grown oxide dots.

3.6.3 Discussion

The resolution of the oxide features is sufficient to create antidot patterns with a period as small as 75 nm. Height and resolution compare favourably with the values reported previously for the LAO of GaSb [28].

The composition of the anodic oxide is not known exactly. While gallium oxide generally occurs as Ga_2O_3, antimony can have different oxidation states and may form Sb_2O_3, Sb_2O_5, or a mixture thereof. While thermal oxidation of GaSb yields a mixture of Ga_2O_3 and Sb_2O_3, the native oxide contains predominantly Ga_2O_3 and Sb_2O_5 [31]. GaSb has a molar volume of approximately $34{\cdot}1\,\mathrm{cm}^{-3}$ [32] and Ga_2O_3 one of $31{\cdot}2\,\mathrm{cm}^{-3}$; the molar densities of Sb_2O_3 and Sb_2O_5 are $52{\cdot}2\,\mathrm{cm}^{-3}$ and $85{\cdot}6\,\mathrm{cm}^{-3}$ respectively [33]. Using these bulk values, one predicts a volume expansion factor between 1·2 for Ga_2O_3/Sb_2O_3 and 1·7 for Ga_2O_3/Sb_2O_5, which is consistent with the range of 1·5 to 2·0 observed experimentally. An oxide mixture containing predominantly Sb_2O_5 appears to be indicated by these calculations, but the volume expansion may be further affected by differences from the bulk crystal structure of the oxides and by incorporation of water.

The sudden changes in the dot shape are related to changes in the geometrical configuration of the actual tip, as is illustrated by the observed 'rubber stamp' effect. The re-

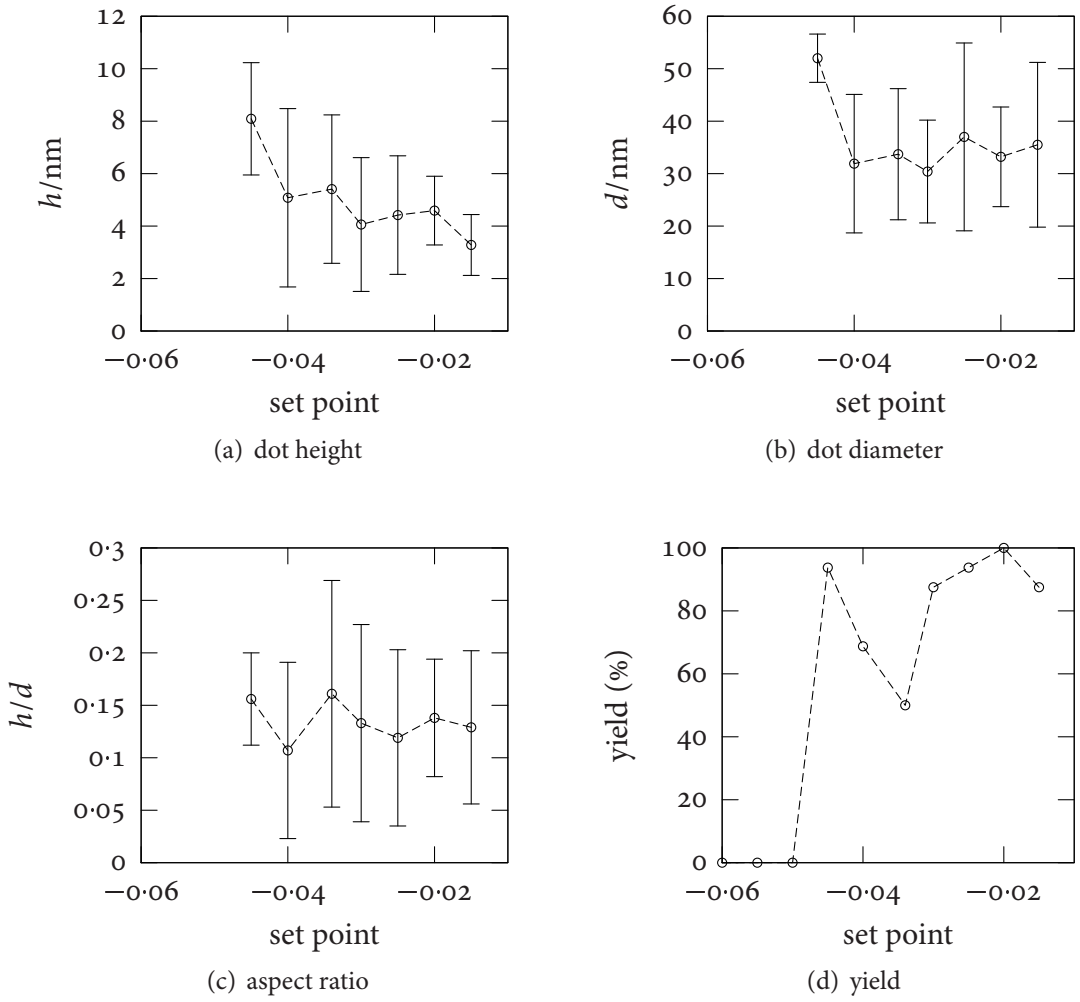

(a) dot height (b) dot diameter

(c) aspect ratio (d) yield

Figure 3.10: Set point dependence of oxide dot growth on GaSb. Oxide dots in a square lattice with lattice constant $a = 300\,\mathrm{nm}$ were grown at 45 % relative humidity by applying a bias of −15 V to the tip for 2 s. Each data point was averaged over 16 dots. The data points have been connected with straight lines to aid visualization.

versibility of this phenomenon, the frequent lack of an effect on the imaging resolution, and the size of the features call into question damage to the tips. Instead I propose that the probes pick up contaminants such as oxide particles from the surface. These contaminants could strongly influence the field distribution and the shape of the water meniscus, while imaging would be affected to a lesser degree if they do not touch the surface or their mechanical coupling to the tip is weak. The surface coating affects the ability of tips to pick up contaminants. Catastrophic tip failure is associated with a noticeable increase in current and can therefore be explained by electric breakdown and damage due to Joule heating. Loss of the ability to create any oxide can be attributed to the formation of a non-conducting layer on the tip by oxidation or contamination: Then most of the voltage is dropped across this layer and the tip–sample potential difference falls below the threshold required for anodization. Metal-coated tips can still be affected as the thin metal film can wear off. Both blunted and oxidized tips may rarely revert to a usable condition if collision with the surface chips off part of the tip and a fresh, sharp apex is exposed.

Central indentations have previously been observed in both dots and lines grown using LAO on different materials [4]. Their origin is not fully understood; an explanation based on tip shape can be excluded as a sufficiently blunt tip would be unable to later resolve the observed indentations, which is not in agreement with experiment. Instead, they are likely to be related to a change in the oxide composition at the centre. This is consistent with the observation of DAGATA *et al.*, who see a similar ring structure in the polarizability of oxide dots even in the absence of a corresponding topographical feature.

The lack of success in forming individual oxide dots that is seen for low humidities and large tip–sample distances does not significantly correlate with a decrease of the size of the oxide features. The total absence of oxide dots on some sites is attributed to a failure to form a water meniscus, which is either caused by a thin or non-uniform water layer on the substrate or a large tip–sample separation when the bias is switched on.

3.7 Local Anodic Oxidation of Thin Aluminium Layers

3.7.1 Overview

I have performed a limited number of experiments to assess the possibility of patterning thin aluminium films using LAO. This allows to use the AFM to create etch masks for reactive ion etching as described in Sec. 4.2.4, thus overcoming the inherent limitation to shallow features.

3.7.2 Performance

Using the procedure employed for the anodization of GaSb surfaces, features could successfully be drawn on thin (7 to 40 nm) aluminium layers created by evaporation on either GaSb or SiO_2. As aluminium rapidly forms a native oxide in contact with air, LAO was performed within a week of evaporation on these samples. For each dot, a pulsed bias of −20 V was applied for 0·5 to 2 s to a conducting silicon tip tracing the sample topography in non-contact mode after disconnecting the feedback loop. For high-quality oxide layers, a reference potential was provided by contacting the metallization separately.

In this way, large dot arrays could be created with good reproducibility as illustrated in Fig. 3.11. The smallest dot diameters and largest dot heights that could reliably be realized were 100±10 nm and 10±1 nm. Individual dots with diameters comparable to those achieved on GaSb could be created. The dot geometry depended on the specific tip used for anodization. The occurrence of repeating features indicated that both the imaging and the lithographic resolution was limited by finite tip size effects.

3.7.3 Oxide Removal

The aluminium oxide created by anodization with the AFM can be etched selectively in a mixture of 85 % phosphoric acid, deionized water, and chromiumtrioxide [24]. Fig. 3.12 shows a cross-section through the same six oxide dots before and after removal of the oxide.

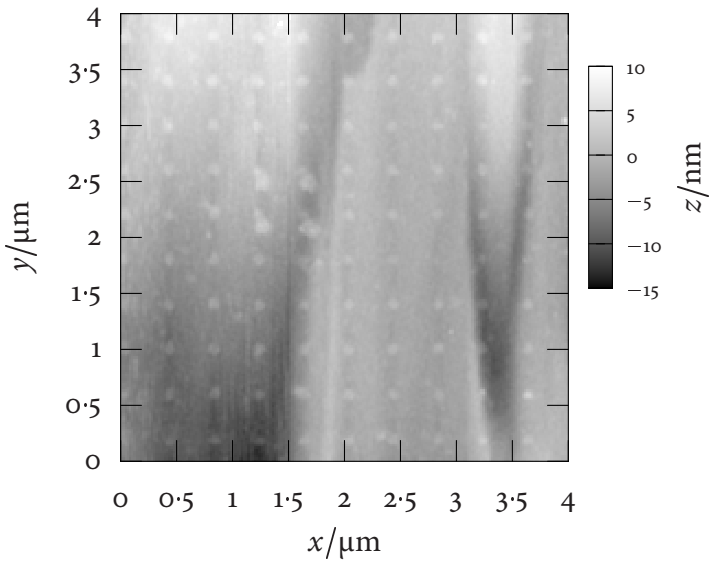

Figure 3.11: AFM micrograph of oxide dots created on aluminium by LAO. The array has a lattice constant of $a = 400\,\text{nm}$. The dots have an average diameter of $120 \pm 20\,\text{nm}$ and a height of $3 \pm 1\,\text{nm}$. They were created using a conducting silicon tip by applying a pulsed bias voltage of $-20\,\text{V}$. The corrugation is caused by the underlying DHET, on which the aluminium was evaporated. The four additional dots near the centre were drawn separately.

Comparatively large oxide dots with a period of 400 nm and a diameter of $140 \pm 10\,\text{nm}$ were chosen to minimize the impact of artifacts caused by a finite tip size, *e.g.*, as a result of incomplete penetration of narrow holes. The oxide dots had a height of $4 \pm 1\,\text{nm}$ and left holes with an estimated depth of $8 \pm 1\,\text{nm}$ and a diameter of $130 \pm 10\,\text{nm}$ after removal of the oxide. It is notable that the holes were much more uniform in their shape and vertical size than the oxide mounds observed before etching. The bottoms of the individual holes appeared flat.

3.7.4 Discussion

Aluminium layers have successfully been patterned in a way analogous to LAO of GaSb. The oxide thickness that has been achieved is similar to the values reported previously [18,24,25]. The lateral resolution is less than either obtained on GaSb in the context of the present work or achieved by a comparable method on Al before [18]. It appears to be limited by finite

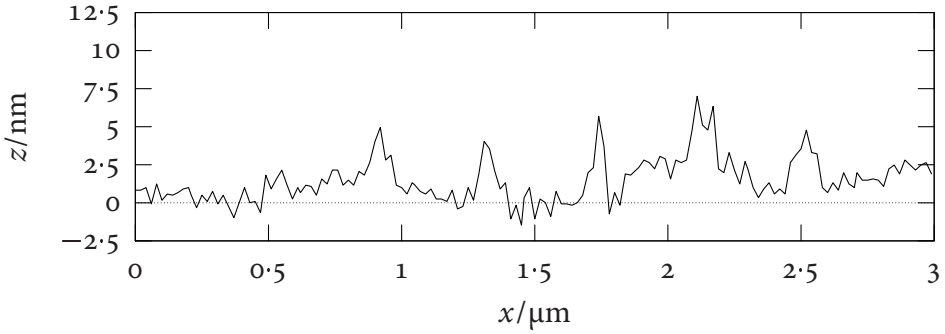

(a) Dots created using LAO

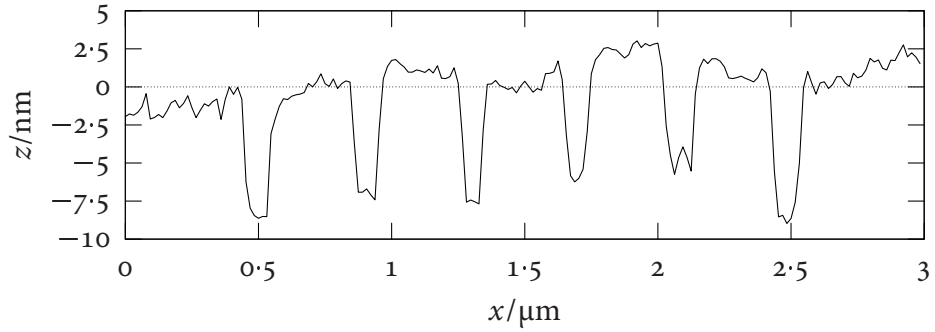

(b) After selective etching of Al_2O_3

Figure 3.12: Removal of oxide dots created on Al using LAO. Both parts show a surface profile of the same region on the sample. The vertical scale is strongly exaggerated, while identical for both plots.

tip size, even though the same tips are capable of producing smaller features on GaSb. One possible explanation for this is the roughness of the surface on the scale of the radius of the tip apex, which may allow a larger meniscus to form or promote the contamination of the tip by small oxide particles.

According to Eq. (3.11), a hole depth $b_2 \approx 4 \pm 1\,\mathrm{nm}$ corresponding to a dot height $b_1 \approx 8 \pm 1\,\mathrm{nm}$ indicates a volume expansion factor qv_o/v_m of $1{\cdot}5 \pm 0{\cdot}2$, which agrees with the results reported for similar experiments in the literature [18, 24]. Aluminium generally occurs in a single oxidation state, and aluminium (III) oxide has a molar volume of $v_o \approx 25{\cdot}5\,\mathrm{cm}^{-3}$, while solid aluminium has a molar volume of $v_m \approx 10{\cdot}0\,\mathrm{cm}^{-3}$ [33]. Since the chemical formula for aluminium (III) oxide is Al_2O_3, $q = 0{\cdot}5$ and the expected volume expansion factor

for full oxidation is approximately 1·3. Given the uncertainty of the experimental value, this is in reasonable agreement with the observation. However, a different experimental volume expansion can also be attributed to a difference in the structure of the anodic oxide from bulk α-Al_2O_3; in particular, water may be incorporated during oxidation. The presence of a native oxide prior to anodization does not affect this argument, provided the selective oxide removal is performed soon after the LAO step. The native oxide layer is removed in the etch and the remaining hole reflects the volume of metal actually anodized. After the etch, the metal will oxidize again, but the effect on the hole shape is small if the measurement is performed immediately. As the maximal achievable oxide height is approximately 10 nm, complete oxidation of aluminium layers up to 20 nm should be possible.

3.8 Conclusions

An attempt has been made to elucidate the underlying principle of local anodic oxidation (LAO), which uses the electric field created by the negatively biased tip of an SPM to enhance the migration of ions through a native oxide layer and thus locally cause further oxidation. I have also reviewed previous attempts at LAO, which illustrate the fundamental capabilities of the method, especially its ability to modify semiconductor surfaces with a resolution comparable to electron beam lithography (EBL). Considerations for using the technique in the creation of regular dot patterns have been put forward.

I have evaluated LAO of several III–V semiconductors and metals, with a focus on Al and especially GaSb because of their intended use in sample fabrication. The importance of the shape and configuration of the tip apex for lithographic performance has been pointed out, and explanations for failure modes have been suggested. It has been noted that reliability can be improved by modulating the bias voltage. On GaSb and Al, the origin of the observed mounds from oxidation has been conclusively verified by selectively removing the oxide in a suitable etchant and showing that holes remained that possessed a depth compatible with the expected volume expansion.

I have shown that AFM lithography on GaSb surfaces is able to produce oxide dot arrays with lattice periods of less than $a = 75\,\text{nm}$ (Fig. 3.4). The feature size can be as small as 30 nm and oxide heights of up to 10 nm can be achieved. On thin aluminium layers created by evaporation on GaSb or SiO_2, a minimal feature size of 130 nm has been realized. Aluminium films with a thickness of up to 20 nm can in principle be oxidized completely, opening up holes in the layer after oxide removal.

In summary, LAO using an AFM is a lithographic technique that combines a high resolution with features that make it attractive for prototyping. The required instruments are highly accessible and allow for a variety of *in situ* monitoring techniques, most importantly an imaging mode that is independent of the exposure mechanism. Many interesting systems can be modified directly with little or no damage to the surrounding areas. However, LAO suffers from a relatively poor repeatability and reliability, being reliant on a well-defined AFM tip, a condition that can often not be fulfilled as variation between different tips and changes in the tip during operation are quite evident. Moreover, the technique is limited to very shallow modifications of materials that naturally form thin stable oxide films in the presence of oxygen. These restrictions may be circumvented by using a separate sensitive layer and a means of pattern transfer, but in doing so some advantages of the method, especially its simplicity and non-invasiveness may be negated.

Bibliography

[1] J. A. Dagata, J. Schneir, H. H. Harary, C. J. Evans, M. T. Postek, and J. Bennett. Modification of hydrogen-passivated silicon by a scanning tunneling microscope operating in air. *Applied Physics Letters*, 56(20):2001–2003, May 1990.

[2] A. E. Gordon, R. T. Fayfield, D. D. Litfin, and T. K. Higman. Mechanisms of surface anodization produced by scanning probe microscopes. *Journal of Vacuum Science and Technology*, 13(6):2805–2808, November/December 1995.

[3] M. Calleja, J. Anguita, R. García, K. F. Pérez-Murano, and J. A. Dagata. Nanometre-scale oxidation of silicon surfaces by dynamic force microscopy: reproducibility, kinetics and nanofabrication. *Nanotechnology*, 10:34–38, 1998.

[4] J. A. Dagata, T. Inoue, J. Itoh, K. Matsumoto, and H. Yokoyama. Role of space charge in scanned probe oxidation. *Journal of Applied Physics*, 84(12):6891–6900, December 1998.

[5] P. M. Campbell, E. S. Snow, and P. J. McMarr. AFM-based fabrication of Si nanostructures. *Physica B*, 227:315–317, 1996.

[6] A. Dorn, M. Sigrist, A. Fuhrer, T. Ihn, T. Heinzel, K. Ensslin, W. Wegscheider, and M. Bichler. Electric properties of antidot lattices fabricated by atomic force lithography. *Applied Physics Letters*, 80(2):252–254, January 2002.

[7] N. F. Mott. The theory of the formation of protective oxide films on metals.—III. *Transactions of the Faraday Society*, 43:429–434, 1947.

[8] N. Cabrera and N. F. Mott. Theory of the oxidation of metals. *Reports on Progress in Physics*, 12:163–184, 1948.

[9] A. T. Fromhold, Jr. Metal oxidation kinetics from the viewpoint of a physicist: The microscopic motion of charged defects through oxides. *Langmuir*, 3(6):886–896, 1987.

[10] R. Vullers. *Oxidation of Titanium Films with an Atomic Force Microscope*. PhD thesis, Katholieke Universiteit Leuven, 2000.

[11] N. F. Mott. A theory of the formation of protective oxide films on metals. *Transactions of the Faraday Society*, 35:1175–1177, 1939.

[12] N. F. Mott. The theory of the formation of protective oxide films on metals, II. *Transactions of the Faraday Society*, 39:472–483, 1940.

[13] Z. Shen, S. Hou, H. Sun, X. Zhao, and Z. Xue. Local oxidation of titanium thin films using an atomic force microscope under static and pulsed voltages. *Journal of Physics D: Applied Physics*, 37:1357–1361, May 2004.

[14] H. J. Song, M. J. Rack, K. Abugharbieh, S. Y. Lee, V. Khan, D. K. Ferry, and D. R. Allee. 25 nm chromium oxide lines by scanning tunneling lithography in air. *Journal of Vacuum Science and Technology B*, 12(6):3720–3724, November/December 1994.

[15] P. A. Fontaine, E. Dubois, and D. Stiévenard. Characterization of scanning tunneling microscopy and atomic force microscopy-based techniques for nanolithography on hydrogen-passivated silicon. *Journal of Applied Physics*, 84(4):1776–1781, August 1998.

[16] F. Pérez-Murano, G. Abadal, N. Barniol, X. Aymerich, J. Servat, P. Gorostiza, and F. Sanz. Nanometer-scale oxidation of Si(100) surfaces by tapping mode atomic force microscopy. *Journal of Applied Physics*, 78(11):6797–6801, December 1995.

[17] S. Belaidi, P. Girard, and G. Lévêque. Electrostatic forces acting on the tip in atomic force microscopy: Modelization and comparison with analytic expressions. *Journal of Applied Physics*, 81(3):1023–1030, February 1996.

[18] Z. J. Davis, G. Abadal, O. Hansen, X. Borisé, B. Barnibol, F. Pérez-Murano, and A. Boisen. AFM lithography of aluminum for fabrication of nanomechanical systems. *Ultramicroscopy*, 97:467–472, 2003.

[19] G. A. C. Jones. Private communication, 2002.

[20] T. Hattori, Y. Ejiri, K. Saito, and M. Yasutake. Fabrication of nanometer-scale structures using atomic force microscope with conducting probe. *Journal of Vacuum Science and Technology A*, 12(4):2586–2590, July/August 1994.

[21] T. Fayfield and T. K. Higman. Fabrication and transport measurements of atomic force microscope modified silicon metal–oxide–semiconductor field-effect transistors. *Journal of Vacuum Science and Technology B*, 13(3):1285–1289, May/June 1995.

[22] E. S. Snow and P. M. Campbell. AFM-fabrication of sub-10-nanometer metal-oxide devices with in situ control of electrical properties. *Science*, 270(5242):1639–1641, December 1995.

[23] R. Nemutudi, N. J. Curson, N. J. Appleyard, D. A. Ritchie, and G. A. C. Jones. Modification of a shallow 2DEG by AFM lithography. *Microelectronic Engineering*, 57–58:967–973, 2001.

[24] A. Boisen, K. Birkelund, O. Hansen, and F. Grey. Fabrication of submicron suspended structures by laser and atomic force microscopy lithography on aluminum combined with reactive ion etching. *Journal of Vacuum Science and Technology B*, 16(6):2977–2981, November/December 1998.

[25] G. Abadal, A. Boisen, Z. J. Davis, O. Hansen, and F. Grey. Combined laser and atomic force microscope lithography on aluminum: Mask fabrication for nanoelectromechanical systems. *Applied Physics Letters*, 74(21):3206–3208, 1999.

[26] N. J. Curson, R. Nemutudi, N. J. Appleyard, M. Pepper, D. A. Ritchie, and G. A. C. Jones. Ballistic transport in a GaAs/$Al_xGa_{1-x}As$ one-dimensional channel fabricated using an atomic force microscope. *Applied Physics Letters*, 78(22):3466–3468, May 2001.

[27] U. F. Keyser, H. W. Schumacher, U. Zeitler, R. J. Haug, and K. Eberl. Fabrication of quantum dots with scanning probe nanolithography. *physica status solidi (b)*, 224(3):681–684, 2001.

[28] S. Sasa, T. Ikeda, A. Kajiuchi, and M. Inoue. AFM fabrication and characterisation of InAs/AlGaSb nanostructures. *Solid-State Electronics*, 42(7–8):1069–1073, 1998.

[29] S. Sasa, A. Nakashima, S. Yodogawa, T. Kita, and M. Inoue. Magnetotransport properties of InAs nanostructure devices produced by AFM oxidation. *Physica B*, 314:95–98, 2002.

[30] S. Sasa, A. Nakashima, Y. Nakajima, and M. Inoue. Aharonov–Bohm oscillations observed in nanoscale open-dot structures fabricated in an InAs surface inversion layer. *Physica E*, 20:224–227, 2004.

[31] K. Möller, L. Töben, Z. Kollonitsch, C. Giesen, M. Heuken, F. Willig, and T. Hannappel. In-situ monitoring and analysis of GaSb(100) substrate deoxidation. *Applied Surface Science*, 242(392–398), 2005.

[32] Ioffe Physico-Technical Institute. New semiconductor materials. characteristics and properties. http://www.ioffe.rssi.ru/SVA/NSM/, November 2005.

[33] M. Winter. WebElements periodic table. http://www.webelements.com/, November 2005.